Article

The black hole low-mass X-ray binary V404 Cygni is part of a wide triple

https://doi.org/10.1038/s41586-024-08120-6

Received: 4 April 2024

Accepted: 25 September 2024

Published online: 23 October 2024

Check for updates

Kevin B. Burdge[1,2]✉, Kareem El-Badry[3], Erin Kara[1,2], Claude Canizares[1,2], Deepto Chakrabarty[1,2], Anna Frebel[1,2], Sarah C. Millholland[1,2], Saul Rappaport[1,2], Rob Simcoe[1,2] & Andrew Vanderburg[1,2]

Evidence suggests that, when compact objects such as black holes and neutron stars form, they may receive a 'natal kick', during which the stellar remnant gains momentum. Observational evidence for neutron star kicks is substantial[1,2], yet is limited for black hole natal kicks, and some proposed black hole formation scenarios result in very small kicks[3–5]. Here we report that the canonical black hole low-mass X-ray binary (LMXB) V404 Cygni is part of a wide hierarchical triple with a tertiary companion at least 3,500 astronomical units (AU) away from the inner binary. Given the orbital configuration, the black hole probably received a sub-5 km s^{-1} kick to have avoided unbinding the tertiary. This discovery lends support to the idea that at least some black holes form with nearly no natal kick. Furthermore, the tertiary in this system lends credence to evolutionary models of LMXBs involving a hierarchical triple structure[6]. Remarkably, the tertiary is evolved, indicating that the system formed 3–5 billion years ago and that the black hole has removed at least half a solar mass of matter from its evolved secondary companion. During the event in which the black hole formed, it is required that at least half of the mass of the black hole progenitor collapsed into the black hole; it may even have undergone a complete implosion, enabling the tertiary to remain loosely bound.

Black holes are the stellar remnants of the most massive stars. Gravitational-wave astronomy has raised key questions about the formation of these objects, including the role of natal kicks[7] and dynamical interactions[6,8,9]. There are several proposed formation pathways for these stellar remnants, including some channels in which there is an implosion with no associated natal kicks or supernovae[3,5,10–12]. The best constraints on black hole kick physics come from the galactic orbits of X-ray binaries[13], astrometric microlensing[14] and orbital dynamics[4]. These constraints have largely ruled out the need for kicks >100 km s^{-1} except for in a handful of systems with exceptional orbits[15,16].

We report the discovery that the black hole X-ray binary V404 Cygni, the first LMXB widely accepted to host a black hole (with a black hole mass of $9^{+0.2}_{-0.6}\,M_{\odot}$ (ref. 17)), is part of a wide hierarchical triple. Our serendipitous discovery originated from examining an optical image of V404 Cygni on the Aladin Lite tool[18], illustrated in Fig. 1a, and noting that there is a nearby star just 1.43 arcsec from V404 Cygni with Gaia proper motions matching those of V404 Cygni, as seen in Fig. 1b. We investigated the proper motions of nearby sources and, in Fig. 2a, show that such a chance agreement in proper motions is unlikely. In Fig. 2c, we quantify the probability of such an alignment occurring by chance, which we find is about 10^{-7} (Methods). While searching the literature on V404 Cygni, we found several works that commented on the nearby star, with most simply assuming that it was an interloper[19,20]. One notable exception was Maitra et al.[21], who speculated "in passing whether the blended star is truly unrelated to the V404 system" owing to the similar estimated distance and extinction of the blended star. V404 Cygni was noted as having a peculiar velocity in a previous work[22] and this was attributed to a kick. As part of our astrometric analysis, we investigated nearby stars and found that the velocity of V404 Cygni is typical of stars in the vicinity (Methods).

Given the 1.43-arcsec separation and estimated distance of 2.39 ± 0.15 kpc (ref. 22), we find that the wide tertiary companion is at least 3,500 AU away from the inner binary, which corresponds to a Keplerian velocity of just a few kilometres per second. As illustrated in Fig. 1a,c, this separation is approximately 90 times larger than the distance of Pluto to the Sun and 25,000 times larger than that of the inner V404 Cygni binary, which has a separation of just 0.14 AU, less than half the distance between the Sun and Mercury.

To further confirm this association, we analysed archival Very Large Telescope (VLT) X-shooter spectroscopic observations (which targeted V404 Cygni but contained a spatially resolved trace of the tertiary) and obtained further follow-up Gemini Multi-Object Spectrographs (GMOS) spectroscopy of the source (Methods). We conducted a radial velocity analysis and found excellent agreement with the reported systemic velocity of V404 Cygni. As seen in the histogram of radial velocities of nearby stars shown in Fig. 2c, this is unlikely to have occurred by chance, further solidifying the association of the two components.

We fit the spectroscopic observations with model atmospheres, focusing on the region around the Hα and Hβ absorption lines in the GMOS spectra (Methods), and the region around the calcium triplet lines in the X-shooter observations, shown in Fig. 3d. As well as fitting the spectroscopic observations with model atmospheres, we

[1]Department of Physics, Massachusetts Institute of Technology, Cambridge, MA, USA. [2]Kavli Institute for Astrophysics and Space Research, Massachusetts Institute of Technology, Cambridge, MA, USA. [3]Division of Physics, Mathematics and Astronomy, California Institute of Technology, Pasadena, CA, USA. ✉e-mail: kburdge@mit.edu

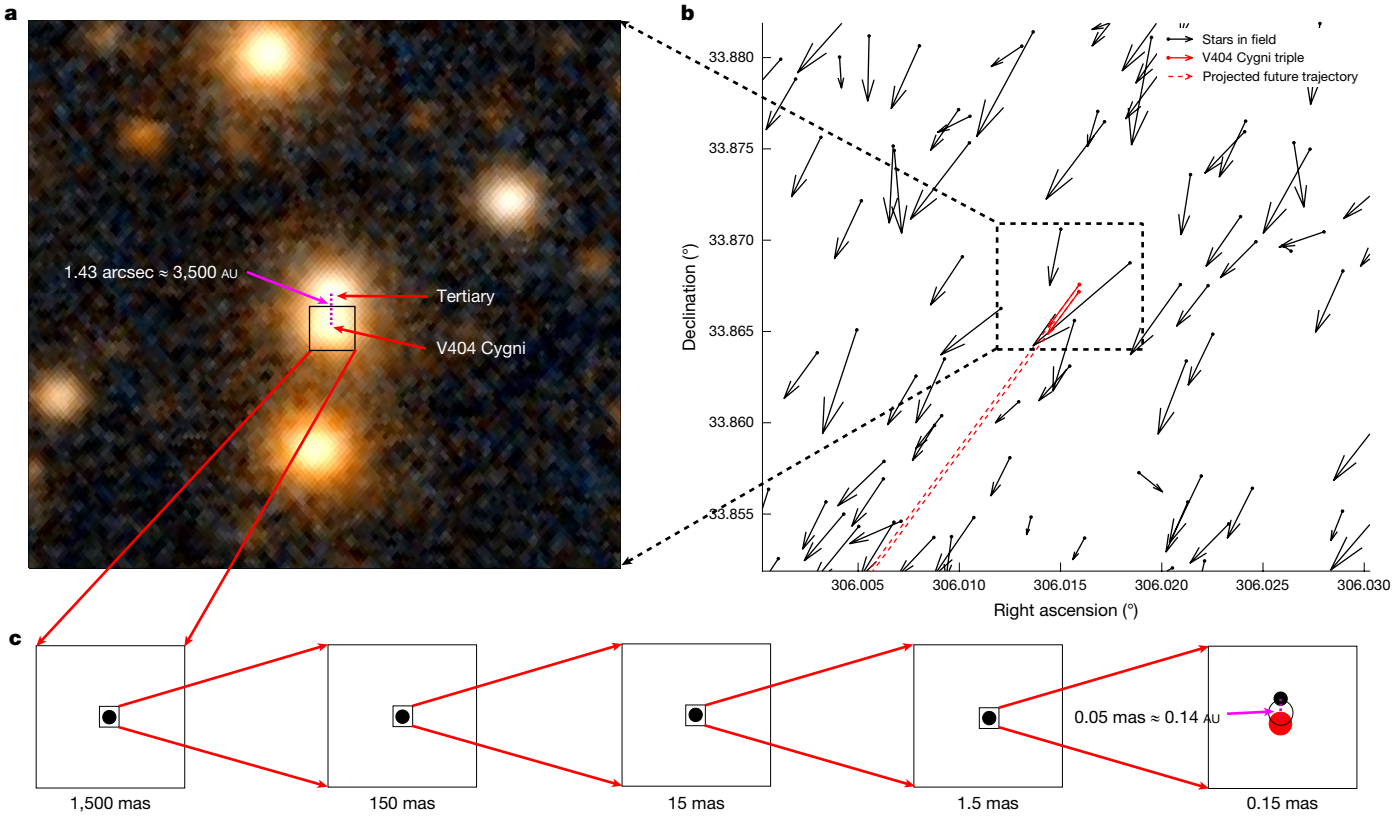

Fig. 1 | Astrometric configuration of V404 Cygni. a, Pan-STARRS image of V404 Cygni and its companion, shown using the Aladin interface, with V404 Cygni and the tertiary labelled in red and the separation of 1.43 arcsec indicated in magenta. We discovered the tertiary while viewing the source on Aladin and inspecting the Gaia astrometry on the interface, finding strong agreement in the measured proper motions of these two sources. **b**, Plot of the positions and proper motion vectors of all stars in the field, with V404 Cygni and its tertiary indicated in red. **c**, Zoom-in on the inner binary of V404 Cygni, showing the 2.5×10^4 ratio of the semimajor axes of the inner and outer orbits in the triple.

also fit the broadband spectral energy distribution (SED), carefully extracting photometry by modelling the point spread function (PSF) in epochal Panoramic Survey Telescope and Rapid Response System (Pan-STARRS) images of the source owing to the blending of the tertiary and V404 Cygni (Methods). Furthermore, we use archival Hubble Space Telescope observations to obtain a measurement in the near-ultraviolet at 330 nm and archival observations with the NIRC2 instrument of the Keck observatory to measure the near-infrared flux at approximately 2 microns. By jointly fitting the spectra and SED, we obtained constraints on the temperature, metallicity and radius, with values reported in Fig. 3c.

One notable result in our modelling of the SED and spectra is that we find that the tertiary in V404 Cygni has started to evolve off of the main sequence and is about twice its initial radius. By fitting the tertiary with MIST isochrones shown in Fig. 3a, we find that this constrains the age of the system to about 3–5 Gyr and the mass of the tertiary to around 1.2 solar masses (our full parameter estimates can be found in Fig. 3c).

The secondary of V404 Cygni, like the donors seen in some other black hole LMXBs, exhibits enhanced lithium abundance, and this has been attributed to formation as a result of accretion processes onto the black hole or in the supernova that formed it[23]. Given our constraint on the age of the system, we can rule out that this lithium abundance is a result of recent formation; however, we inspected our X-shooter and GMOS spectra and concluded that, at this time, there is insufficient signal to noise and resolution to determine whether the tertiary has enhanced lithium.

To learn about the physical constraints imposed on the formation of the black hole, we simulated the dynamics of the triple with a range of configurations, accounting for the black hole kick, mass lost during the black hole formation and the initial orbital periods of the secondary and the tertiary, to investigate which black hole formation scenarios could retain the loosely bound tertiary.

As seen in Fig. 4a, the only way the inner binary could have experienced a large kick and retained the tertiary is if the tertiary started at a short orbital period and was sent into a highly eccentric orbit reaching >3,500 AU at apastron owing to a kick to the inner binary. This scenario is unlikely, as we would need to fine-tune the kick to the inner system to be large but just barely below the escape velocity of the system (Methods). We find that scenarios in which the tertiary started in a wide orbit, and the inner binary received a small kick of just a few kilometres per second, are thus strongly favoured.

When considering the inner binary, we simulated two scenarios. In one case, we allowed the secondary to start in a wide orbit between 100 AU and 300 AU. This scenario is viable for reproducing the current system, as we find that von Zeipel–Lidov–Kozai cycles could readily cause the secondary to migrate into its current 6.4-day orbit (Methods). As illustrated by the red histograms in Fig. 4b, we find that, in this scenario, the black hole kick was probably smaller than 3 km s^{-1} and that the mass lost in the black hole formation could have been up to about 10 solar masses, or about half the mass of the inner binary.

Alternatively, we consider a scenario in which the secondary had an orbital period between 1 and 6 days at black hole formation (its current orbit is 6.4 days). These simulations are illustrated as the blue histograms in Fig. 4b. In this case, the barycentre of the inner binary receives a substantial Blaauw kick[24] as a result of mass loss, even if the black hole itself does not receive a kick. This results from matter being ejected symmetrically in the rest frame of the black hole progenitor, ejecting it from the binary with a net asymmetric velocity equal to the orbital velocity of the black hole in the barycentric frame. At orbital periods on the order of days, the black hole orbits with a velocity of

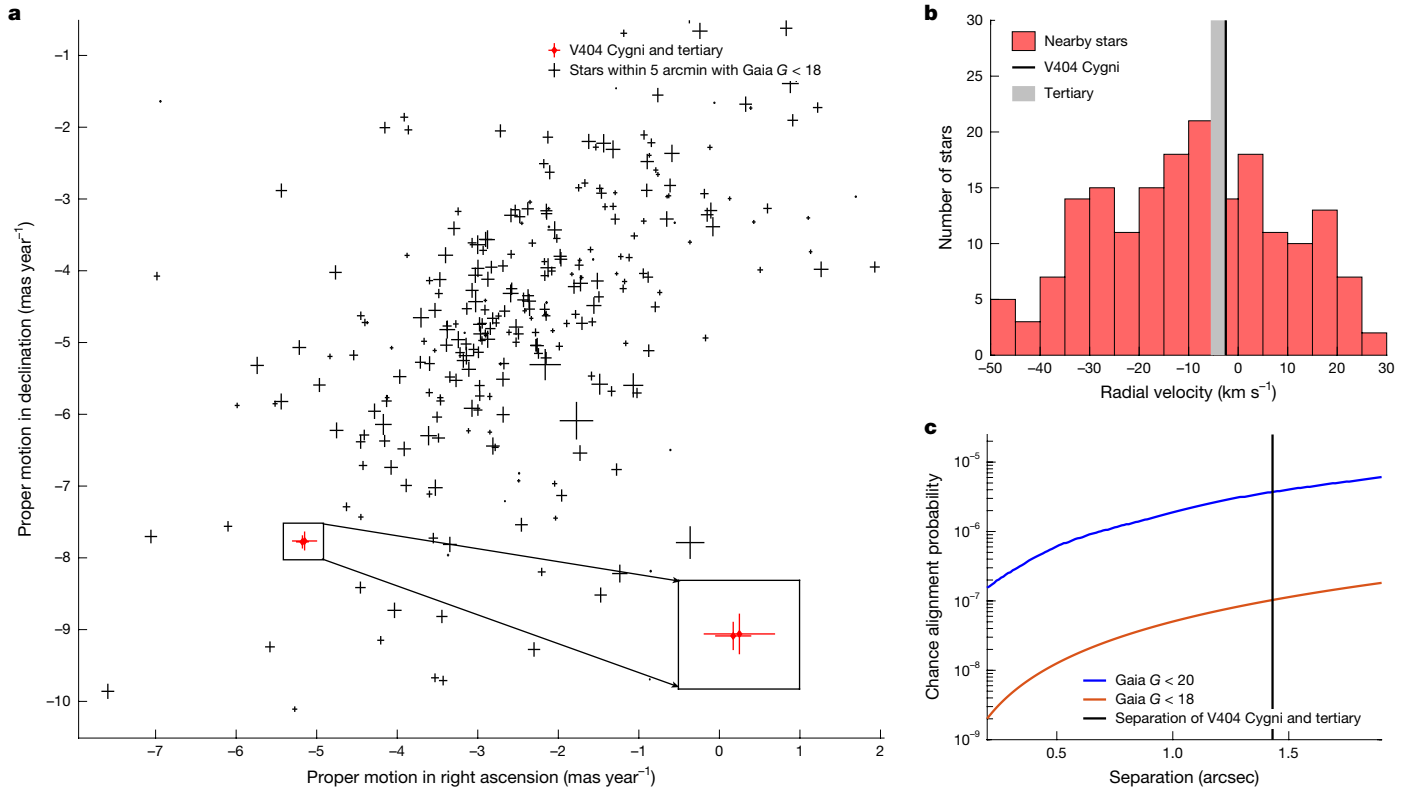

Fig. 2 | Probabilistic analysis of astrometric alignment. a, Plot illustrating the proper motions of all Gaia stars brighter than 18th magnitude within 5 arcmin of V404 Cygni and the strong agreement between V404 Cygni and its tertiary (shown in red). **b**, Histogram of Gaia-measured radial velocities of stars in the vicinity of V404 Cygni, with the systemic velocity of V404 Cygni shown as the black vertical line and the measured radial velocity of the tertiary shown as the grey vertical line. **c**, Plot illustrating the chance alignment probability as a function of separation for stars brighter than 18th magnitude (shown in red) and 20th magnitude (shown in blue). This probability accounts for both the agreement in proper motions as well as radial velocity.

a few tens of kilometres per second and, thus, as seen in Fig. 4b, this scenario strongly constrains any possible mass loss during the black hole formation, because even if the black hole does not receive a kick, the inner binary does as a consequence of the mass loss, ejecting the tertiary. One curiosity of this scenario is that, in fine-tuned cases, one can achieve slightly larger black hole kicks while keeping the tertiary bound, because the velocity imparted on the barycentre of the inner binary by mass loss can absorb the effect of the kick oriented in the opposite direction, resulting in a relatively low net kick to the inner binary, allowing the retention of the tertiary. Overall, this scenario still favours small kick velocities of less than 5 km s^{-1} and does not allow for more than about a solar mass to be ejected. Thus, if the secondary started in a tight orbit of a few days, the most probable black hole formation scenario is one in which there was a near-complete implosion of the progenitor star, with negligible mass loss.

In either scenario, a black hole formation event in which there is a complete implosion and no kick always results in the survival of the system. We cannot rule out mass loss in the system but we find it improbable that more than half the mass of the black hole progenitor was suddenly ejected during its formation.

We consider it unlikely that the system formed dynamically in a dense environment such as a globular cluster or the Galactic Centre and was ejected, as the escape velocities of these environments exceed the orbital velocity of the tertiary by an order of magnitude (the young age of the tertiary also disfavours an origin in a globular cluster). We also find it unlikely that the system captured the tertiary in the field as a result of the low cross-section of such an interaction occurring. One possibility is that dynamical capture occurred when the system was part of an open cluster that has since evaporated[25]. We note that the tertiary may have widened its orbit over several billion years as a result of a dynamical scattering into a wide orbit[26]. Although the effects of these two scenarios on kick constraints are difficult to quantify owing to the large number of degrees of freedom, they could potentially allow for larger black hole kicks on formation.

The presence of a tertiary companion in one of the most well-known LMXBs supports theoretical work that has suggested that hierarchical triples may be key to forming black hole LMXBs. Forming black hole LMXBs through purely binary evolution has been theoretically challenging because of the large mass ratios involved, resulting in a common envelope event that proceeds to a merger rather than a successful ejection of the envelope. Thus, theoretical modelling of the formation of such systems has explored the possibility that wide tertiary companions helped the donor migrate into a tight orbit after the formation of the black hole[6]. This is achieved through a gravitational interaction of the tertiary with the inner orbit, known as a von Zeipel–Lidov–Kozai cycle, in which the inner orbit cycles between an inclined and an eccentric orbit. We note that models such as those presented in ref. 6 predict tertiary companions in orbits at roughly 10^4 AU, which is consistent with what we observe in V404 Cygni. One plausible evolutionary scenario for V404 Cygni is that the inner binary began its life with a separation of about 10^2 AU and, over time, Kozai–Lidov cycles drove this to a shorter orbit as a result of tidal dissipation and magnetic breaking draining orbital angular momentum from the inner binary during the highly eccentric phase. Finally, the inner binary hardened to an orbit of <6.5 days, too long for Roche-lobe overflow, whereas the secondary was on the main sequence, but as the secondary evolved, it overflowed its Roche lobe. This is essentially the giant sub-channel described in ref. 6.

We note that searches for wide binary companions are, in general, highly incomplete. To be detected by Gaia, a companion must be: (1) brighter than $G \approx 20.7$ and (2) separated from the inner binary by at least about 1 arcsec (depending on the flux ratio). For V404 Cygni, this corresponds to detection limits of $M \gtrsim 0.9\ M_\odot$ for main-sequence stars

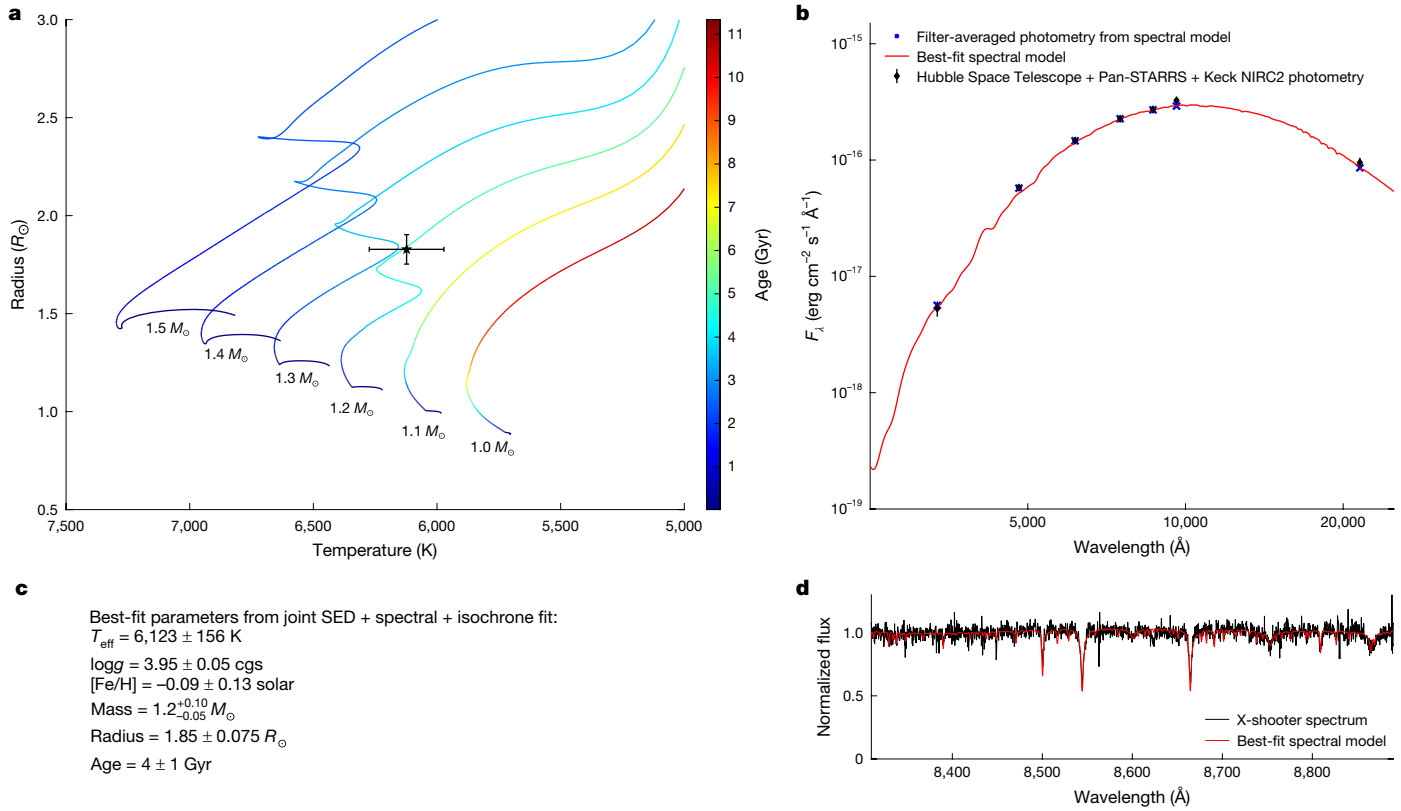

Fig. 3 | Stellar characterization of V404 Cygni tertiary. a, MIST stellar isochrones, with the colour bar indicating the age of stars evolving according to these isochrones. The black star with error bars indicates the position of the tertiary, which overlaps with tracks in the range 1.2–1.3 solar masses at ages of around 3–5 Gyr. **b**, SED of the tertiary in V404 Cygni (black diamonds), with the bluest point coming from Hubble Space Telescope ACS observations, the reddest point from Keck NIRC2 observations and the remaining photometric measurements from Pan-STARRS images. The red curve shows our best-fit spectrum to these data and the blue crosses indicate the filter-averaged flux values from this spectrum. **c**, Our derived parameters as a result of the models illustrated in this figure. **d**, The X-shooter spectrum of the calcium triplet absorption features and other nearby absorption lines in the tertiary (black) and our best-fit spectral model to it (red).

and separations $s \gtrsim 2{,}500$ AU. The separation distribution of solar-type tertiaries peaks at 10–100 AU, with companions at 100–2,500 AU outnumbering those at >2,500 AU by a factor of two[27,28]. Although the separation distribution of tertiaries to massive stars is uncertain, this suggests that companions too close to be detected by Gaia may be common and could have evaded detection so far. Indeed, several black hole LMXBs are thought to have unresolved companions, which have, so far, been interpreted as chance alignments[29–31]. Proper motions for these companions have not yet been measured.

V404 Cygni is nearer and brighter in the optical than most other black hole LMXBs. If the system were approximately 50% more distant, the companion would be blended with the inner binary and Gaia would not have been able to measure its proper motion. If the companion were ≳10% more massive, it would already be a faint white dwarf below the detection limit of Gaia. If it were ≳40% less massive, it would be a main-sequence star below the Gaia detection limit; if it were ≳20% less massive, it would be too faint for Gaia to have measured a precise proper motion and establish the association with high confidence. These considerations all suggest that harder-to-detect tertiaries may well be hiding around other known black holes. It is possible that most black hole LMXBs formed through triple evolution, and deeper searches around other black holes hold promise to detect them.

Evidence suggests that the spin axis of the black hole in V404 Cygni is misaligned from the orbital plane owing to the rapidly changing orientation of the jets in the system, and this has been attributed to a natal kick[32]. However, the presence of the tertiary largely rules out a natal kick. An alternative possibility is that the von Zeipel–Lidov–Kozai cycles induced this misalignment, as the inner orbit would have evolved through a range of inclinations and may have hardened at an inclination misaligned with the original orbit[33,34]. If the current spin of the black hole in the system was primarily inherited from the progenitor star, this could naturally lead to a misalignment of this spin axis with the current orbital plane. However, the evolved 1.2-solar-mass tertiary implies that the black hole has removed at least 0.5 solar masses from the 0.7-solar-mass secondary—which was originally more massive than the tertiary, as it evolved first.

The tertiary companion of V404 Cygni has provided favourable evidence for the formation of at least some LMXBs in hierarchical triples. Moreover, the wide orbit of this object has provided one of the strongest empirical constraints on natal kicks[35] in the formation of a black hole by indicating that the black hole in V404 Cygni probably formed with a kick of less than 5 km s^{-1}, demonstrating that at least some stellar-mass black holes form without substantial natal kicks. We conclude by noting that our simulations strongly suggest that the secondary of V404 Cygni either started in a wider orbit, and migrated in as a result of von Zeipel–Lidov–Kozai interactions, or—if the secondary originated in a tight orbit—the 9-$M_\odot$ black hole formed without ejecting more than a solar mass of matter—a near-complete implosion.

Online content

Any methods, additional references, Nature Portfolio reporting summaries, source data, extended data, supplementary information, acknowledgements, peer review information; details of author contributions and competing interests; and statements of data and code availability are available at https://doi.org/10.1038/s41586-024-08120-6.

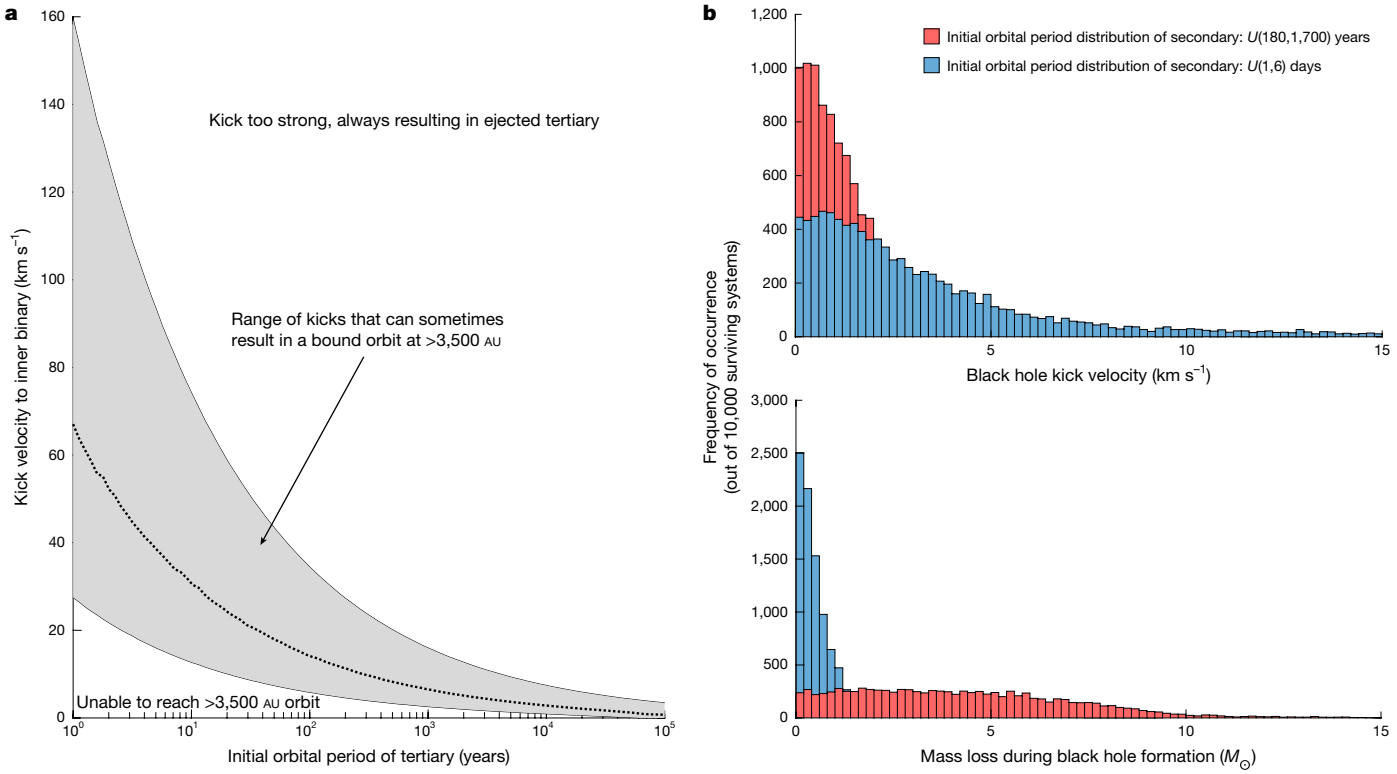

Fig. 4 | Simulation of possible black hole natal kicks in V404 Cygni. **a**, Illustration of the range of possible kick velocities to the inner binary that could result in a bound tertiary at a separation greater than 3,500 AU. In general, large kicks are only allowed if the tertiary originated at a very short orbital period, a scenario that is unlikely to retain the tertiary (Methods). **b**, Histograms representing our simulations of black hole kicks and mass loss in the system. The red histograms represent a scenario in which the secondary originates at a wide range of orbital periods and the blue histograms represent a scenario in which the secondary formed the black hole at very short orbital periods.

1. Hobbs, G., Lorimer, D. R., Lyne, A. G. & Kramer, M. A statistical study of 233 pulsar proper motions. *Mon. Not. R. Astron. Soc.* **360**, 974–992 (2005).
2. Tauris, T. M. et al. Formation of double neutron star systems. *Astrophys. J.* **846**, 170 (2017).
3. Fryer, C. L. & Kalogera, V. Theoretical black hole mass distributions. *Astrophys. J.* **554**, 548–560 (2001).
4. Shenar, T. et al. An X-ray-quiet black hole born with a negligible kick in a massive binary within the Large Magellanic Cloud. *Nat. Astron.* **6**, 1085–1092 (2022).
5. Burrows, A., Wang, T., Vartanyan, D. & Coleman, M. S. B. A theory for neutron star and black hole kicks and induced spins. *Astrophys. J.* **963**, 63 (2024).
6. Naoz, S., Fragos, T., Geller, A., Stephan, A. P. & Rasio, F. A. Formation of black hole low-mass X-ray binaries in hierarchical triple systems. *Astrophys. J. Lett.* **822**, L24 (2016).
7. Callister, T. A., Farr, W. M. & Renzo, M. State of the field: binary black hole natal kicks and prospects for isolated field formation after GWTC-2. *Astrophys. J.* **920**, 157 (2021).
8. O'Leary, R. M., Meiron, Y. & Kocsis, B. Dynamical formation signatures of black hole binaries in the first detected mergers by LIGO. *Astrophys. J. Lett.* **824**, L12 (2016).
9. Rodriguez, C. L., Haster, C.-J., Chatterjee, S., Kalogera, V. & Rasio, F. A. Dynamical formation of the GW150914 binary black hole. *Astrophys. J. Lett.* **824**, L8 (2016).
10. Fryer, C. L. Mass limits for black hole formation. *Astrophys. J.* **522**, 413–418 (1999).
11. Mirabel, F. The formation of stellar black holes. *New Astron. Rev.* **78**, 1–15 (2017).
12. Chan, C., Müller, B., Heger, A., Pakmor, R. & Springel, V. Black hole formation and fallback during the supernova explosion of a 40 $M_{\odot}$ star. *Astrophys. J. Lett.* **852**, L19 (2018).
13. Mandel, I. Estimates of black hole natal kick velocities from observations of low-mass X-ray binaries. *Mon. Not. R. Astron. Soc.* **456**, 578–581 (2016).
14. Andrews, J. J. & Kalogera, V. Constraining black hole natal kicks with astrometric microlensing. *Astrophys. J.* **930**, 159 (2022).
15. Fragos, T. et al. Understanding compact object formation and natal kicks. II. The case of XTE J1118 + 480. *Astrophys. J.* **697**, 1057–1070 (2009).
16. Dashwood Brown, C., Gandhi, P. & Zhao, Y. On the natal kick of the black hole X-ray binary H 1705-250. *Mon. Not. R. Astron. Soc. Lett.* **527**, L82–L87 (2024).
17. Khargharia, J., Froning, C. S. & Robinson, E. L. Near-infrared spectroscopy of low-mass X-ray binaries: accretion disk contamination and compact object mass determination in V404 Cyg and Cen X-4. *Astrophys. J.* **716**, 1105–1117 (2010).
18. Bonnarel, F. et al. The ALADIN interactive sky atlas. A reference tool for identification of astronomical sources. *Astron. Astrophys. Suppl. Ser.* **143**, 33–40 (2000).
19. Udalski, A. & Kaluzny, J. CCD photometry of the X-ray nova V404 Cygni after the 1989 outburst. *Publ. Astron. Soc. Pac.* **103**, 198 (1991).
20. Casares, J., Charles, P. A., Jones, D. H. P., Rutten, R. G. M. & Callanan, P. J. Optical studies of V404 Cyg, the X-ray transient GS2023+338 – I. The 1989 outburst and decline. *Mon. Not. R. Astron. Soc.* **250**, 712–725 (1991).
21. Maitra, D. et al. Simultaneous multiwavelength observations of V404 Cygni during its 2015 June outburst decay strengthen the case for an extremely energetic jet-base. *Astrophys. J.* **851**, 148 (2017).
22. Miller-Jones, J. C. A. et al. The first accurate parallax distance to a black hole. *Astrophys. J. Lett.* **706**, L230–L234 (2009).
23. Martin, E. L., Rebolo, R., Casares, J. & Charles, P. A. High lithium abundance in the secondary of the black-hole binary system V404 Cygni. *Nature* **358**, 129–131 (1992).
24. Blaauw, A. On the origin of the O- and B-type stars with high velocities (the "run-away" stars), and some related problems. *Bull. Astron. Inst. Neth.* **15**, 265 (1961).
25. Rozner, M. & Perets, H. B. Born to be wide: the distribution of wide binaries in the field and soft binaries in clusters. *Astrophys. J.* **955**, 134 (2023).
26. Reipurth, B. & Mikkola, S. Formation of the widest binary stars from dynamical unfolding of triple systems. *Nature* **492**, 221–224 (2012).
27. Raghavan, D. et al. A survey of stellar families: multiplicity of solar-type stars. *Astrophys. J. Suppl. Ser.* **190**, 1–42 (2010).
28. Tokovinin, A. From binaries to multiples. II. Hierarchical multiplicity of F and G dwarfs. *Astron. J.* **147**, 87 (2014).
29. Armas Padilla, M. et al. Multiwavelength spectroscopy of the black hole candidate MAXI J1813-095 during its discovery outburst. *Mon. Not. R. Astron. Soc.* **485**, 5235–5243 (2019).
30. Mata Sánchez, D. et al. Dynamical confirmation of a stellar mass black hole in the transient X-ray dipping binary MAXI J1305-704. *Mon. Not. R. Astron. Soc.* **506**, 581–594 (2021).
31. Hynes, R. I., Haswell, C. A., Chaty, S., Shrader, C. R. & Cui, W. The evolving accretion disc in the black hole X-ray transient XTE J1859+226. *Mon. Not. R. Astron. Soc.* **331**, 169–179 (2002).
32. Miller-Jones, J. C. A. et al. A rapidly changing jet orientation in the stellar-mass black-hole system V404 Cygni. *Nature* **569**, 374–377 (2019).
33. Liu, B. & Lai, D. Spin–orbit misalignment of merging black hole binaries with tertiary companions. *Astrophys. J. Lett.* **846**, L11 (2017).
34. Su, Y., Lai, D. & Liu, B. Spin-orbit misalignments in tertiary-induced binary black-hole mergers: theoretical analysis. *Phys. Rev. D* **103**, 063040 (2021).
35. Igoshev, A. P. & Perets, H. B. Wide binary companions to massive stars and their use in constraining natal kicks. *Mon. Not. R. Astron. Soc.* **486**, 4098–4113 (2019).

Methods

Astrometric association

We investigated the robustness of the astrometric association of the tertiary with the inner binary by analysing a sample of all Gaia sources within 30 arcmin of V404 Cygni. In Gaia DR3, there are 80,739 sources in this region of the sky. This corresponds to a source density of 0.0079 sources per square arcsecond. As an initial check, we parsed these 80,739 sources for objects with proper motion values that fall within 1 sigma of V404 Cygni's values and found only 21 such sources. When we account for the error bars of not just V404 Cygni's measured proper motions but also of all other sources, we find that 1,256 sources have 1 sigma confidence intervals that overlap the 1 sigma confidence interval of V404 Cygni. However, the mean magnitude in this sample is Gaia G of 20.5 and thus it is dominated by sources with large uncertainties in proper motions, meaning that the well-measured proper motion of V404 Cygni is consistent with more than 1,000 poorly measured proper motions in this region.

To construct the curve shown in Fig. 2c, which we define as the probability of finding a source within a given separation radius that has proper motions in right ascension and declination consistent within 1 sigma, as well as a radial velocity consistent to within 1 sigma, we take the list of 80,739 Gaia sources within 30 arcmin and further downselect to 39,577 sources with a Gaia G magnitude greater than 20 (to construct the blue curve) and 10,798 sources with a Gaia G magnitude greater than 18 (to construct the red curve). We follow the procedure outlined in ref. 36 to determine whether two sources have consistent proper motions, accounting for possible orbital motion influencing the astrometric solution, requiring that the scalar proper motion difference, $\Delta\mu = \left[\left(\mu^*_{\alpha,1} - \mu^*_{\alpha,2}\right)^2 + \left(\mu_{\delta,1} - \mu_{\delta,2}\right)^2\right]^{-1/2}$, is less than the possible proper motion difference resulting from orbital motion, $\Delta\mu_{\rm orbit}$ plus the uncertainty in the difference, $\sigma_{\Delta\mu} = \frac{1}{\Delta\mu}\left[\left(\sigma^2_{\mu^*_{\alpha,1}} + \sigma^2_{\mu^*_{\alpha,2}}\right)\Delta\mu^2_\alpha + \left(\sigma^2_{\mu_{\delta,1}} + \sigma^2_{\mu_{\delta,2}}\right)\Delta\mu^2_\delta\right]^{-1/2}$. We find that, for stars with Gaia $G > 18$ (the tertiary of V404 Cygni is 17.9), there are only three sources within 30 arcmin that have proper motions consistent with V404 Cygni (this number ranges from 2 to 4 sources, as the number of sources consistent with the proper motions of V404 Cygni depends on the assumed separation, as this is used to compute possible variance in proper motions owing to the orbital motion). In any case, this leads to small chance alignment probabilities. Extended Data Table 1 lists the Gaia astrometric solution of V404 Cygni and its tertiary.

We also consider the radial velocity of the sources in computing the chance alignments. To do this, we selected all Gaia sources within 30 arcmin of V404 Cygni with a Gaia radial velocity error less than 5 km s^{-1} (this is comparable with our measured uncertainty on the radial velocity of the tertiary). We used these sources to construct the histogram in Fig. 2b. From this distribution, we computed that there is an approximately 8.1% probability of a source with a well-measured radial velocity being consistent with that of V404 Cygni to within 1 sigma and we incorporated this information in our chance alignment probabilities illustrated in Fig. 2c.

To translate these numbers into formal chance alignment probabilities, we ask what is the probability that such a source would fall within a circle of some radius (represented by the x axis in Fig. 2c) around V404 Cygni. We use the vertical black line to denote the location of the actual tertiary, which is 1.43 arcsec away from V404 Cygni. A 1.43-arcsec region represents just 1/1584429th of the 30-arcmin region we queried for sources and thus the probability of any individual source falling by chance into such a region is 6.3×10^{-7}. Thus, if we consider the three sources with Gaia $G > 18$ that have proper motions consistent with V404 Cygni, accounting for possible orbital motion at a 1.43-arcsec separation, the probability of one of those sources falling within 1.43 arcsec of V404 Cygni is 1.89×10^{-6}, and when we account for the probability of the radial velocity agreeing to within 1 sigma, this becomes approximately 10^{-7}.

During analysis of the astrometry of V404 Cygni and its tertiary, we used the astrometry of nearby stars to investigate the peculiar velocity reported in ref. 22. Using stars within 1° of V404 Cygni, with similar distances (parallax values between 1/3 and 1/2) and radial velocity errors of less than 5 km s^{-1}, we constructed the Toomre diagram shown in Extended Data Fig. 1 and found that the Gaia astrometry and radial velocities of nearby stars are largely consistent with that of V404 Cygni. The local sample of stars shows v_z values of -4 ± 17 km s^{-1}, consistent with V404 Cygni's v_z value of 5 km s^{-1}.

Constraining kicks and mass loss

To constrain the possible natal kicks the black hole could have received while still retaining the tertiary, we treated the system as a triple with component masses of $M_{\rm BH} = 8.5\,M_\odot$ as the post-supernova black hole mass, $M_2 = 1.5\,M_\odot$ as the initial mass of the inner donor star and $M_3 = 1.2\,M_\odot$ as the initial mass of the tertiary.

We consider four free parameters in our simulations: the initial orbital period of the tertiary, the orbital period of the secondary at black hole formation, the amount of mass ejected in the supernova and the kick that the black hole received. We marginalized over the kick angle and the orientation of the inner binary with respect to the orbit of the outer tertiary and, in all cases, we assumed initially circular orbits and we used an isotropic distribution to describe the inclinations and kick angles. In all cases, we assume that the initial orbits are circular. To determine whether the post-kick orbits remain bound, we follow the procedure outlined in ref. 37, which we outline here. We define a non-dimensional characteristic mass:

$$\widetilde{m} = \frac{M_1 + M_2}{M_1' + M_2}, \tag{1}$$

in which M_1 and M_2 are the initial masses in the system and M_1' is the post-supernova mass of component that underwent mass loss. We also compute a dimensionless ratio of the magnitude of the kick velocity to orbital velocity:

$$\tilde{v} = \frac{v_{\rm kick}}{v_{\rm orb}}, \tag{2}$$

in which $v_{\rm orb}$ is the relative orbital velocity of the two components computed using Kepler's laws (in the case of the inner binary, the two components are the black hole progenitor and the secondary, and in the case of the outer orbit, the components are the tertiary and the centre of mass of the inner binary).

Following ref. 37, this yields a post-supernova energy in the new centre of mass frame given by:

$$E' = -\frac{GM_1'M_2}{2a}\left[2 - \widetilde{m}\left(1 + 2\tilde{v}\cos\phi\cos\theta + \tilde{v}^2\right)\right], \tag{3}$$

in which ϕ and θ represent the polar and azimuthal kick angles, respectively. As observed in ref. 37, for the final system to remain bound, E' must be negative, and the final semimajor axis is given by

$$a' = -\frac{GM_1'M_2}{2E'}. \tag{4}$$

In each simulation, we first use the black hole kick and level of mass loss and consider the impact this has on the barycentric velocity, $v_{\rm sys}$, of the inner orbit. We then use this $v_{\rm sys}$ as the input to a calculation to check whether the outer tertiary will remain bound to the inner binary. We compute $v_{\rm sys}$ using the expression given in ref. 37:

$$v_{\rm sys} = \frac{v_{\rm orb}}{M_1' + M_2}\left[\left(\frac{\mu \Delta M_1}{M_1}\right)^2 - 2\frac{\mu \Delta M_1 M_1'}{M_1}\tilde{v}\cos\phi\cos\theta + (M_1'\tilde{v})^2\right]^{1/2}, \quad (5)$$

in which ΔM_1 is the mass lost in the supernova and μ is the reduced mass of the pre-supernova binary, defined as $\mu = \frac{M_1 M_2}{M_1 + M_2}$.

In constructing the histograms shown in Fig. 4b, we consider two cases: one in which the inner companion was in an orbit between 1 and 6 days when the black hole formed (we use a uniform distribution of orbital periods between these two values) and another case in which it started out at an orbital separation between 100 and 300 AU (we also always enforce that the secondary must start out at a shorter orbital period than the tertiary, although in a fine-tuned scenario, we could imagine a dynamical exchange of these two components). In both cases, the initial orbital period of the tertiary is drawn from a uniform distribution between the orbital period of the secondary and 70,000 years. We use 100 AU as a lower bound to ensure that the von Zeipel–Lidov–Kozai timescales were short enough that the secondary would have migrated into its current orbit over the few billion years age of V404 Cygni. We enforce the 300 AU upper bound because, if the orbit were much wider, it would be dynamically unstable. In both scenarios, we drew from uniform distributions for the black hole kick and mass loss during black hole formation, with the black hole kick being drawn from a uniform distribution between 0 km s^{-1} and 300 km s^{-1} and the mass loss being drawn from a uniform distribution ranging from 0 $M_\odot$ to 20 $M_\odot$. We consider 'surviving' solutions to be ones in which the secondary remains bound in an orbit with a semimajor axis less than the final semimajor axis of the tertiary and the tertiary remains bound with a final semimajor axis greater than 3,500 AU.

To construct Fig. 4a, which represents the range of possible kicks the inner binary could have experienced while retaining the tertiary as a function of the initial orbital period of the tertiary, we iterate over initial orbital periods of the tertiary and simply apply a range of systemic velocities to the inner binary, without assuming any mass loss, and investigate which solutions retain the tertiary in a bound orbit greater than 3,500 AU. We find that solutions in which the tertiary started in a tight orbit and is kicked to its current orbit have a low survival rate, as illustrated in Extended Data Fig. 2.

Spectroscopic observations

We searched the European Southern Observatory (ESO) archive for observations of V404 Cygni in which the companion may have serendipitously fallen inside the slit. This yielded a VLT/X-shooter spectrum obtained on 16 July 2015 (programme 295.D-5027; PI: Rahoui), between the main outburst and mini-outburst[38], when the black hole was in quiescence. To our knowledge, these data have not been published elsewhere. As seen in Extended Data Fig. 3a, two separate traces are clearly visible in the raw spectra, separated by about 1.4 arcsec, with one 5–10 times brighter than the other. Because V404 Cygni has no other comparably bright neighbours, there is little doubt that the fainter of the two traces corresponds to the companion. The seeing was about 1.3 arcsec (full width at half maximum, FWHM), meaning that the centre of the companion's trace is separated from V404 Cygni by 2.5 times the 'σ' of the seeing disk. Given that the companion is 5–10 times fainter than V404 Cygni in the VIS data, with its relative flux contribution increasing towards redder wavelengths, the companion was probably only partially in the slit. The data were taken with the 1.2-arcsec slit, yielding a typical resolution of 6,500 in the VIS band.

The mid-exposure time is HJD 2457219.692, when the ephemeris of ref. 38 predicts a radial velocity of −49.9 km s^{-1} for the donor. Twelve separate 148-s exposures were obtained sequentially in nod-and-shuffle mode, for a total exposure time of 1,776 s in the VIS band. After inspecting the 12 exposures, we rejected one in which the companion was unusually faint, presumably because it fell farther outside the slit. We reduced and combined the other 11, for an effective exposure time of 1,628 s in the VIS band. We reduced the data using the ESO Reflex pipeline[39] with standard calibrations. This performs bias subtraction, flat fielding, wavelength calibration using afternoon ThAr arcs and order merging. We set the extraction window for the two sources manually using the 'localize-slit-position' and 'localize-slit-height' parameters. To minimize contamination from V404 Cygni, we extracted only approximately 50% of the companion's trace on the far side of V404 Cygni. The fact that the extracted spectrum of the companion shows no emission in Hα, in which V404 Cygni shows a strong double-peaked emission line (see Extended Data Fig. 3b,c), suggests that there is little contamination.

We used the 'A' and 'B' telluric bands to perform a flexure correction in the wavelength solution, obtaining a −12 km s^{-1} correction with the A band and a −11.0 km s^{-1} correction with the B band, and adopted a correction of −11.5 km s^{-1}, with a systematic uncertainty of −1 km s^{-1}. After applying these corrections, we converted the X-shooter spectrum to air wavelengths and applied the Barycentric correction of 8.6 km s^{-1} in the file headers.

We also obtained an extra spectroscopic observation using GMOS on the 8.1-m Gemini North telescope on Mauna Kea, to determine whether there was any radial velocity variability within the tertiary (programme GN-2023B-DD-105). We used the 0.5-arcsec slit and the R831_G5302 grating, which provides a resolution of approximately 4,400. Our spectrum covered a wavelength range from 4,576 Å to 6,925 Å. Although being slightly lower resolution than the X-shooter data, the spectrum provided a substantially higher signal-to-noise ratio at bluer wavelengths. We illustrate the region around Hβ and Hα in Extended Data Fig. 4a,b.

We aligned the position angle of the slit perpendicular to the angle between V404 Cygni and the tertiary, effectively masking V404 Cygni. The observation was obtained in good seeing (FWHM ≈ 0.7 arcsec), meaning that V404 Cygni was nearly four times the 'σ' of the seeing disk from the nearest edge of the slit, and contamination is expected to be negligible. We used a 900-s exposure, yielding a signal-to-noise ratio of about 30 per pixel at 6,600 Å, about 10 per pixel at 5,600 Å and about 5 per pixel at 5,000 Å. We obtained a CuAr arc on-sky immediately after the science exposure.

We reduced the GMOS data using PypeIt, which required manual construction of a new template for the R831 grating. PypeIt performs bias and flat-field correction, cosmic-ray removal, wavelength calibration, sky subtraction, extraction of 1D spectra and heliocentric radial velocity corrections. Like the X-shooter data, we checked the wavelength solution using the telluric bands and in this case found that no correction was needed.

Radial velocity measurements

We used the X-shooter spectra to measure the radial velocities of both components, as well as perform atmospheric fits in conjunction with modelling the SED. To measure radial velocities, we used the ultranest kernel density estimator to fit an atmospheric model constructed using the PHOENIX stellar atmosphere library[40]. We selected a region between 8,480 Å and 8,700 Å for the fit, as this wavelength range contains the calcium triplet lines, which provide a strong radial velocity signal in the X-shooter spectrum. We allowed the radial velocity to be a free parameter and fixed the other parameters in this atmospheric model to an effective temperature of $T_{\rm eff}$ = 6,100 K, log$g$ = 3.95 cgs and [Fe/H] = 0 based on our joint atmospheric + SED fit. Our fit yielded a radial velocity measurement of $-4.5 \pm 2.5 \pm 1$ km s^{-1} for the tertiary, in excellent agreement with the -2.0 ± 0.4 km s^{-1} systemic velocity of the inner binary reported in ref. 38.

We also conducted a radial velocity analysis of the GMOS spectra, fitting the region between 6,400 Å and 6,700 Å to capture the Hα absorption line and nearby features and the region between 4,750 Å and 5,000 Å for the Hβ absorption feature. We find that

this analysis yields a radial velocity of -4.1 ± 1.9 km s^{-1}, consistent with that of the X-shooter data and of the systemic velocity of V404 Cygni. We note that the orbital motion of the tertiary is on the order of a few kilometres per second and may also introduce some difference between the systemic velocities of the two components at this level.

SED

To model the SED of the tertiary in V404 Cygni, we used a combination of observations obtained with the Pan-STARRS[41], the Advanced Camera for Surveys (ACS)[42] aboard the Hubble Space Telescope and the near-infrared camera (NIRC2) on the W. M. Keck Observatory[43].

Because of the overlapping PSF of V404 Cygni's inner binary and the tertiary in the Pan-STARRS images, we performed our own PSF photometry of the source by constructing a routine using the photutils package to iteratively run over the epochal Pan-STARRS images. We used a small cut-out region, illustrated in Extended Data Fig. 5b, for our analysis, constructing a PSF model using the nearby bright stars near the top and bottom of this cut-out. After constructing the PSF model, we use photutils to identify bright sources in each image and fit for the position of the PSF, as seen in Extended Data Fig. 5c, and found that this yielded good-quality photometry, leaving only small residuals, as seen in Extended Data Fig. 5d. We note that initially when we performed this analysis on the stacked Pan-STARRS images, we were unable to eliminate substantial residuals and discovered after inspecting the epochal images that there was a nearby focal plane artefact, in the shape of a heart, which may have been contaminating some of the stacked images. One example of this artefact is shown in Extended Data Fig. 5a and we found that its position regularly changed at different pointings, sometimes contaminating V404 Cygni or our comparison stars, leading to a variable PSF model over the stacked images. To quantify the uncertainties in the apparent magnitude of the V404 Cygni tertiary, we computed the standard deviation of the estimated apparent magnitude across all epochal Pan-STARRS images for which we were able to perform photometry (in each filter). As well as using the photometric scatter across epochal images to estimate the measurement error, we compared the inferred apparent magnitude using the star just to the north of the triple and the one just to the south of the triple, to quantify the systematic error in each filter. We note that we used the Pan-STARRS1 reference catalogue of apparent magnitudes for our two comparison stars as a basis for calibrating the photometry.

We used an archival Hubble Space Telescope observation (proposal ID: 9686; PI: Hynes) to extract flux in the ACS/HRC F330W filter. These observations consist of two 600-s exposures. As can be seen in Extended Data Fig. 6a, the tertiary is visible and well resolved from V404 Cygni in these images. We used the ACStools Python package to compute the flux of the tertiary, using a 0.2-arcsec aperture and applying the appropriate corrections to the flux to account for the portion of the PSF not encompassed by this aperture.

We performed infrared photometry using a single archival NIRC2 image of V404 Cygni, shown in Extended Data Fig. 6b. We used a 0.5-arcsec aperture to extract flux for the tertiary, as well as a comparison star just to the north of the tertiary. We used the 2MASS reference magnitude of this reference star to calibrate our flux, although we elected to apply a systematic error of 10% to our photometry owing to the difference in filters in the 2MASS system (2MASS K_s) and the K_p filter used in the NIRC2 observation. We elected not to perform more in-depth photometry on the full archive of hundreds of images because we found that this photometric measurement had little overall impact on our results.

Joint SED, spectroscopic and isochrone analysis

We performed an analysis in which we fit the SED with model atmospheres, synthesizing fluxes using the pyphot tool. As well as the SED measurement, the only other measurement we included in this analysis was the estimated radio parallax of 0.418 ± 0.024 to constrain the distance (and appropriately account for the uncertainty in distance in estimating the radius) and the reddening value of $E(g-r) = 1.27$ reported in ref. 44. As with the analysis of the spectra, we used the ultranest kernel density estimate to perform this fit. We fit for four free parameters, the distance, effective temperature, metallicity and radius of the star. This analysis of the SED alone yielded the following parameters: $T_{\rm eff} = 6{,}080 \pm 86$ K, $r = 1.882 \pm 0.047\ R_\odot$, $d = 2.42 \pm 0.14$ kpc and [Fe/H] $= -0.21 \pm 0.28$. We note that these estimates depend strongly on the assumed reddening but are broadly consistent with what we estimate from the spectra.

Data availability

All data used in this publication are available on public telescope archives.

Code availability

On request, the first author will provide code (primarily in Python) used to conduct simulations and compute chance alignment probabilities, as well as code used to construct figures.

36. El-Badry, K. & Rix, H.-W. Imprints of white dwarf recoil in the separation distribution of Gaia wide binaries. *Mon. Not. R. Astron. Soc.* **480**, 4884–4902 (2018).
37. Brandt, N. & Podsiadlowski, P. The effects of high-velocity supernova kicks on the orbital properties and sky distributions of neutron-star binaries. *Mon. Not. R. Astron. Soc.* **274**, 461–484 (1995).
38. Casares, J. et al. Accretion and outflow in V404 Cyg. *Mon. Not. R. Astron. Soc.* **488**, 1356–1365 (2019).
39. Freudling, W. et al. Automated data reduction workflows for astronomy. The ESO Reflex environment. *Astron. Astrophys.* **559**, A96 (2013).
40. Husser, T. O. et al. A new extensive library of PHOENIX stellar atmospheres and synthetic spectra. *Astron. Astrophys.* **553**, A6 (2013).
41. Chambers, K. C. et al. The Pan-STARRS1 surveys. Preprint at https://arxiv.org/abs/1612.05560 (2016).
42. Sirianni, M. et al. The photometric performance and calibration of the Hubble Space Telescope Advanced Camera for Surveys. *Publ. Astron. Soc. Pac.* **117**, 1049–1112 (2005).
43. Matthews, K. & Soifer, B. T. in *Infrared Astronomy with Arrays, The Next Generation* (ed. McLean, I. S.) 239–246 (Springer, 1994).
44. Green, G. M., Schlafly, E., Zucker, C., Speagle, J. S. & Finkbeiner, D. A 3D dust map based on Gaia, Pan-STARRS 1, and 2MASS. *Astrophys. J.* **887**, 93 (2019).

Acknowledgements We dedicate this work to the memory of our dear friend, Tom Marsh. K.B.B. is a Pappalardo Postdoctoral Fellow in Physics at MIT and thanks the Pappalardo fellowship programme for supporting his research. This research was supported by NSF grant AST-2307232. We thank S. Vitale and H. Perets for helpful discussions and suggestions.

Author contributions K.B.B. discovered the tertiary as a result of collaborating with E.K. K.E.-B. obtained spectroscopic observations with GMOS and reduced the GMOS and archival X-shooter spectrum. K.B.B. (with extensive guidance from K.E.-B., who independently conducted several of the analyses) performed spectroscopic modelling of the spectra, estimated chance alignment probabilities, performed isochrone fitting, and kick simulations. K.B.B. wrote the majority of the main text and Methods. K.E.-B. contributed text to both the main text and Methods. E.K. contributed discussions on accretion physics and implications the tertiary has for this. C.C., D.C., A.F., S.C.M., S.R., R.S. and A.V. contributed important ideas throughout the text, including discussion of abundances, implications for kick physics, and the possibility of triple evolution.

Competing interests The authors declare no competing interests.

Additional information
Supplementary information The online version contains supplementary material available at https://doi.org/10.1038/s41586-024-08120-6.

Correspondence and requests for materials should be addressed to Kevin B. Burdge.

Peer review information *Nature* thanks Boaz Katz, Ilya Mandel and David Vartanyan for their contribution to the peer review of this work. Peer reviewer reports are available.

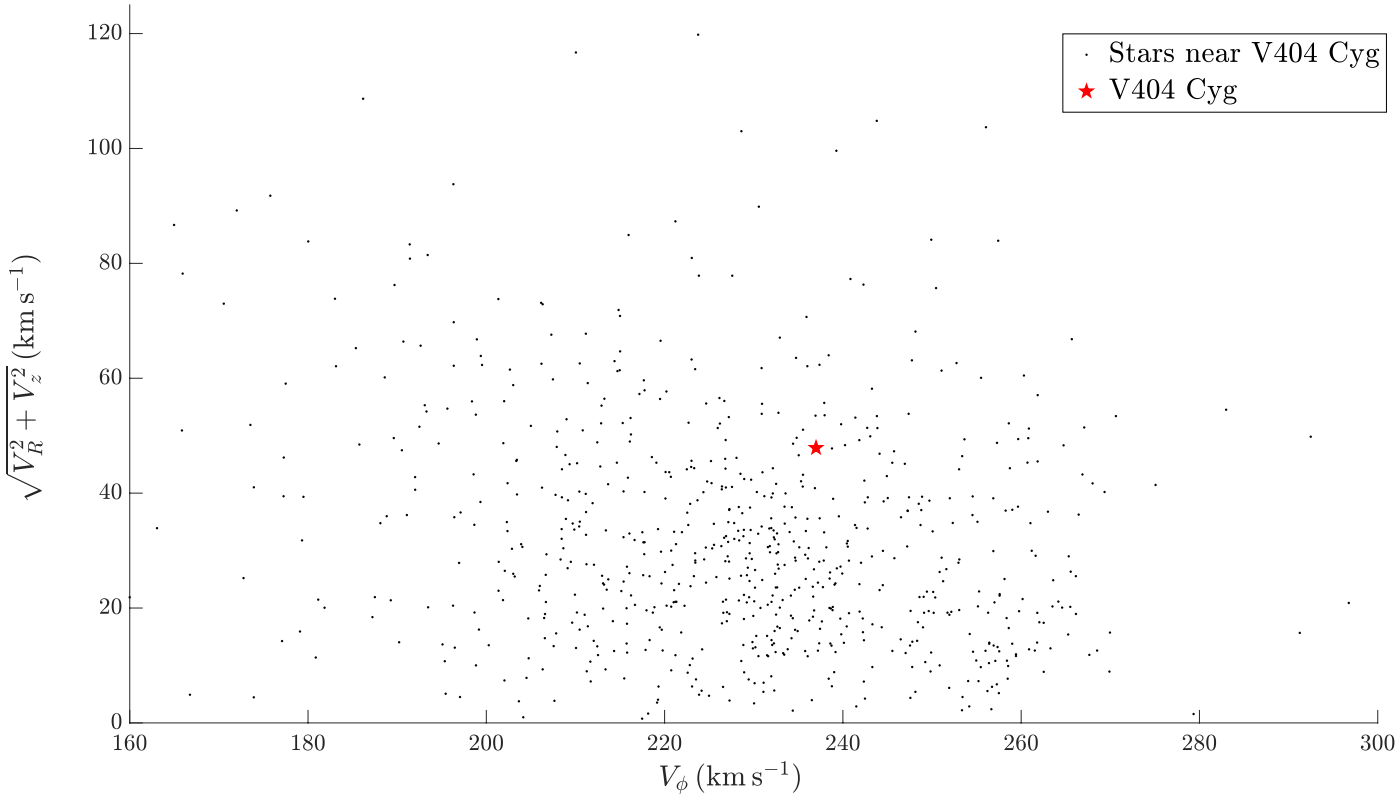

Extended Data Fig. 1 | Toomre diagram of V404 Cygni and nearby stars. Toomre diagram illustrating the galactic orbital velocity of V404 Cygni relative to stars within a degree of V404 Cygni. We find that the velocity of V404 Cygni is largely consistent with nearby stars.

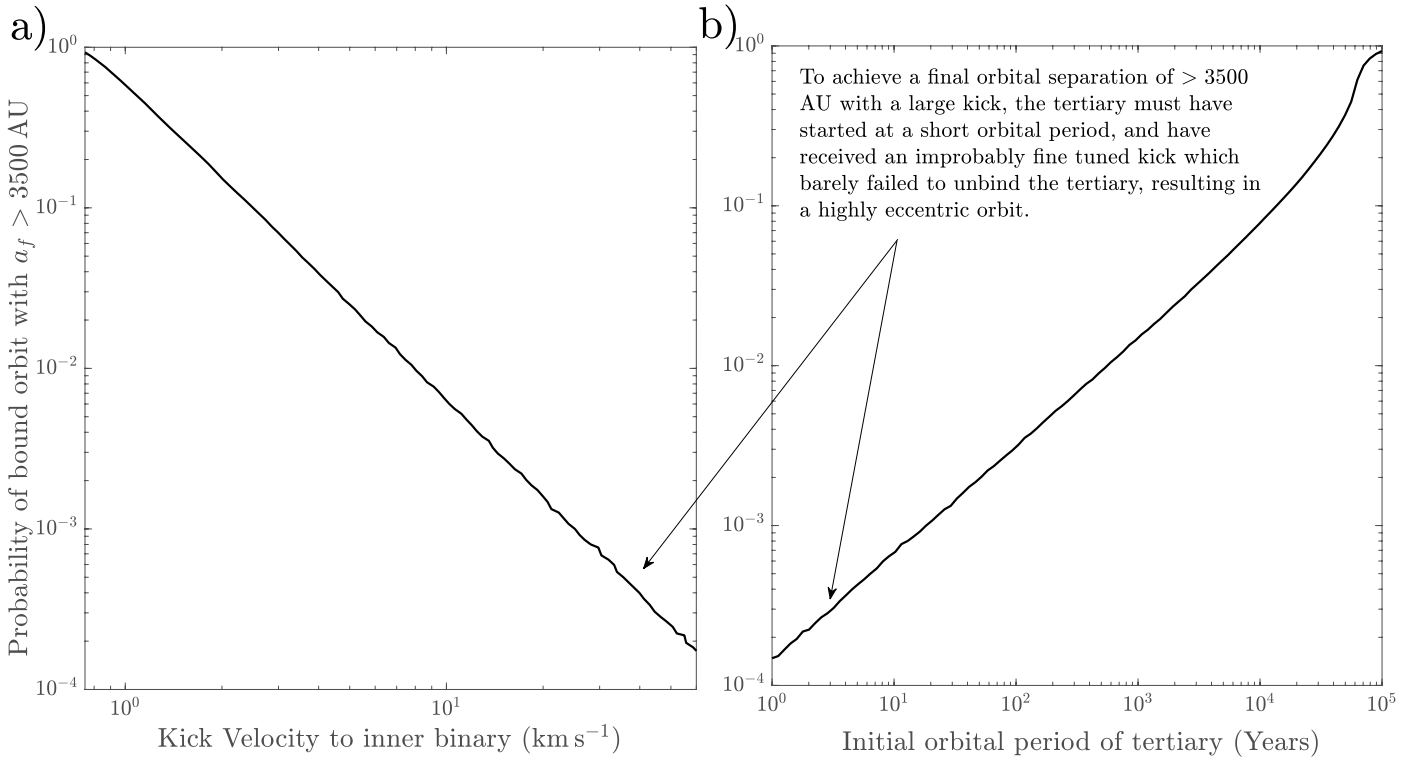

Extended Data Fig. 2 | Kick simulation probabilities of retaining tertiary in wide orbit. a, The probability of retaining a bound tertiary as a function of the kick velocity in the inner binary. In general, this probability diminishes at large kicks because these are only allowed when the tertiary originates in a tight orbit and must be fine-tuned to be large enough to send it to a wide separation without unbinding it. **b**, The probability of retaining a bound tertiary at greater than 3,500 AU as a function of the initial orbital period of the tertiary. These probabilities are diminished for tertiaries that originate in tight orbits as a result of the large amount of fine-tuning required to send the tertiary to such a wide orbit without unbinding it.

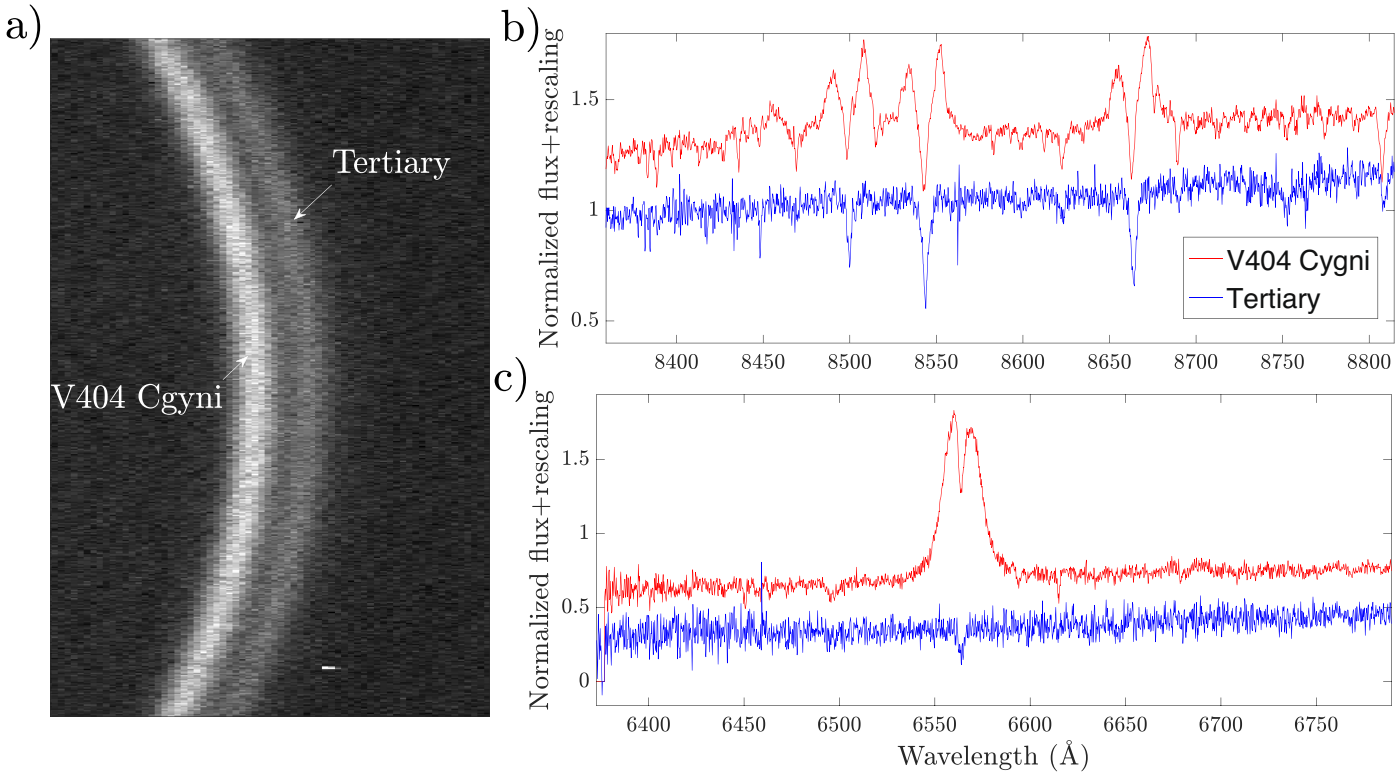

Extended Data Fig. 3 | X-shooter spectrum of V404 Cygni and the tertiary. **a**, A region in the archival X-shooter spectrum of V404 Cygni, with the traces associated with the inner binary of V404 Cygni and the tertiary both labelled. **b**, The extracted X-shooter spectra around the calcium triplet region for V404 Cygni (shown in red) and the tertiary (shown in blue), illustrating that we were able to extract a spectrum of the tertiary with minimal contamination by V404 Cygni. **c**, The spectrum of V404 Cygni (shown in red) and the tertiary (blue) around the Hα absorption line.

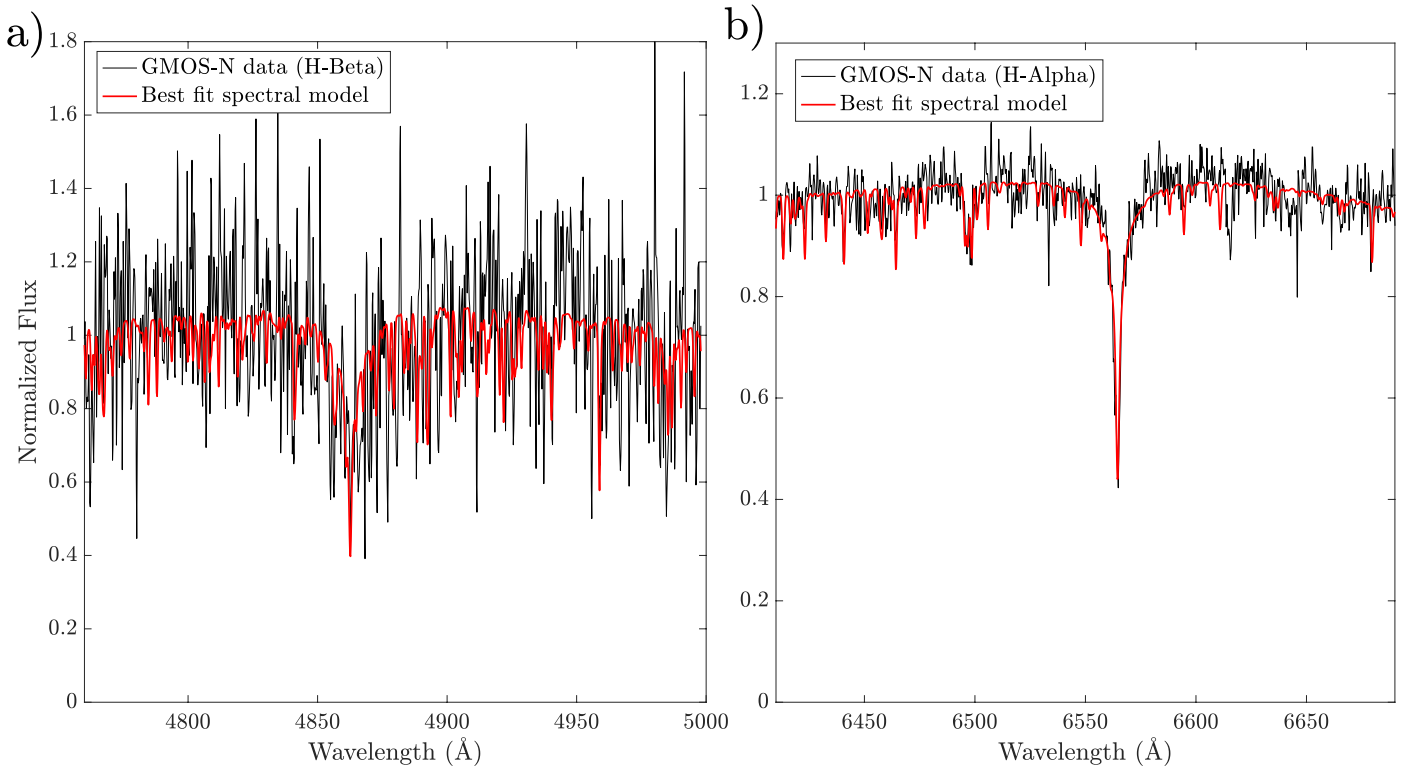

Extended Data Fig. 4 | GMOS-N spectrum of tertiary. a, The Gemini GMOS-N spectrum of the Hβ absorption feature in the tertiary (black) and our best-fit spectral model to it (red). **b**, The Gemini GMOS-N spectrum of the Hα absorption feature in the tertiary (black) and our best-fit spectral model to it (red).

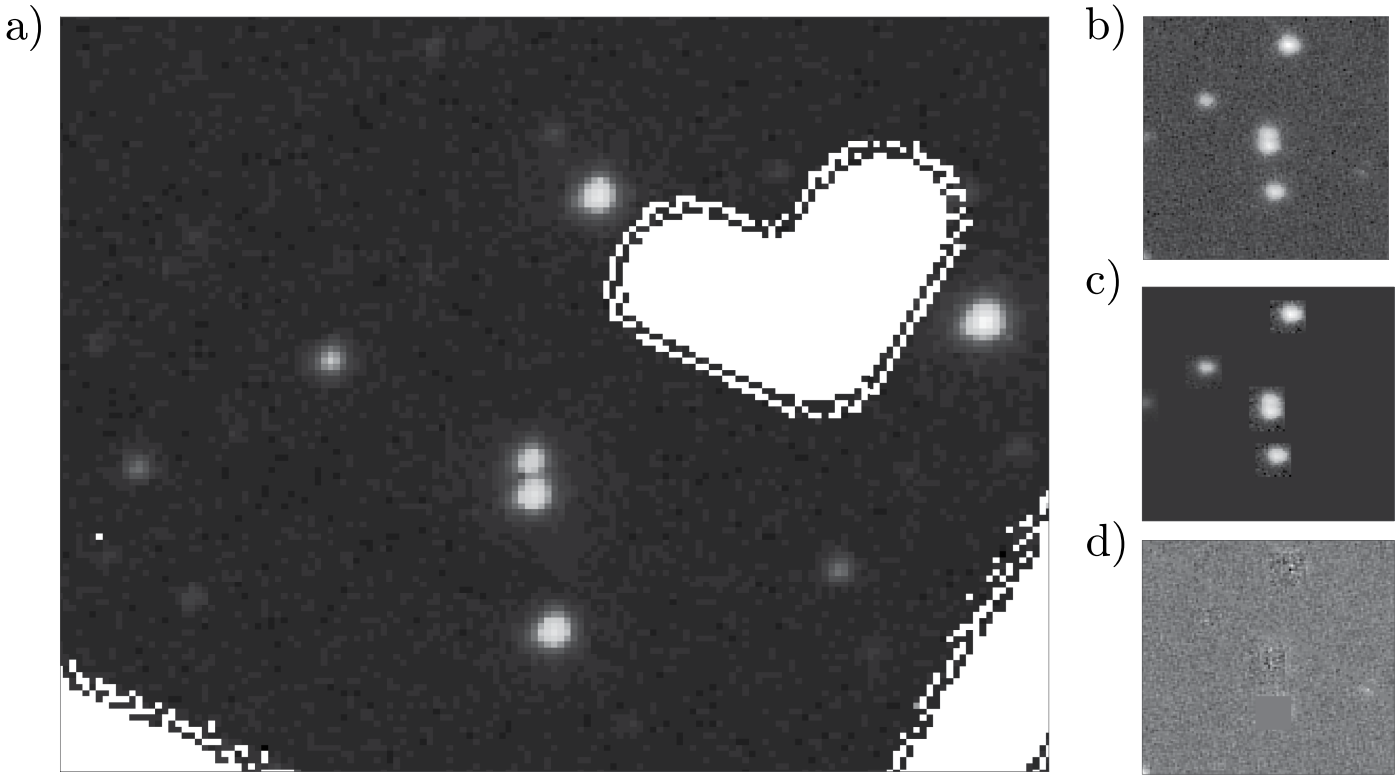

Extended Data Fig. 5 | Pan-STARRS images of V404 Cygni and the tertiary. **a**, An example of a heart-shaped artefact that contaminates many of the Pan-STARRS images of V404 Cygni. We believe that this artefact degraded the quality of the stacked Pan-STARRS images by occasionally occluding either V404 Cygni or comparison stars, resulting in a non-uniform PSF across the stacked images. This is why we ultimately decided to use epochal images as the basis of our photometry. **b**, An epochal Pan-STARRS r-band image of V404 Cygni. We used epochal images such as this to extract fluxes for our SED analysis. **c**, An image illustrating the PSF model we applied to the image to extract photometry for V404 Cygni's tertiary. **d**, A cut-out illustrating the residuals after we extract PSF photometry, with the PSF model constructed using the bottom star in the image (hence the zero residuals around this star).

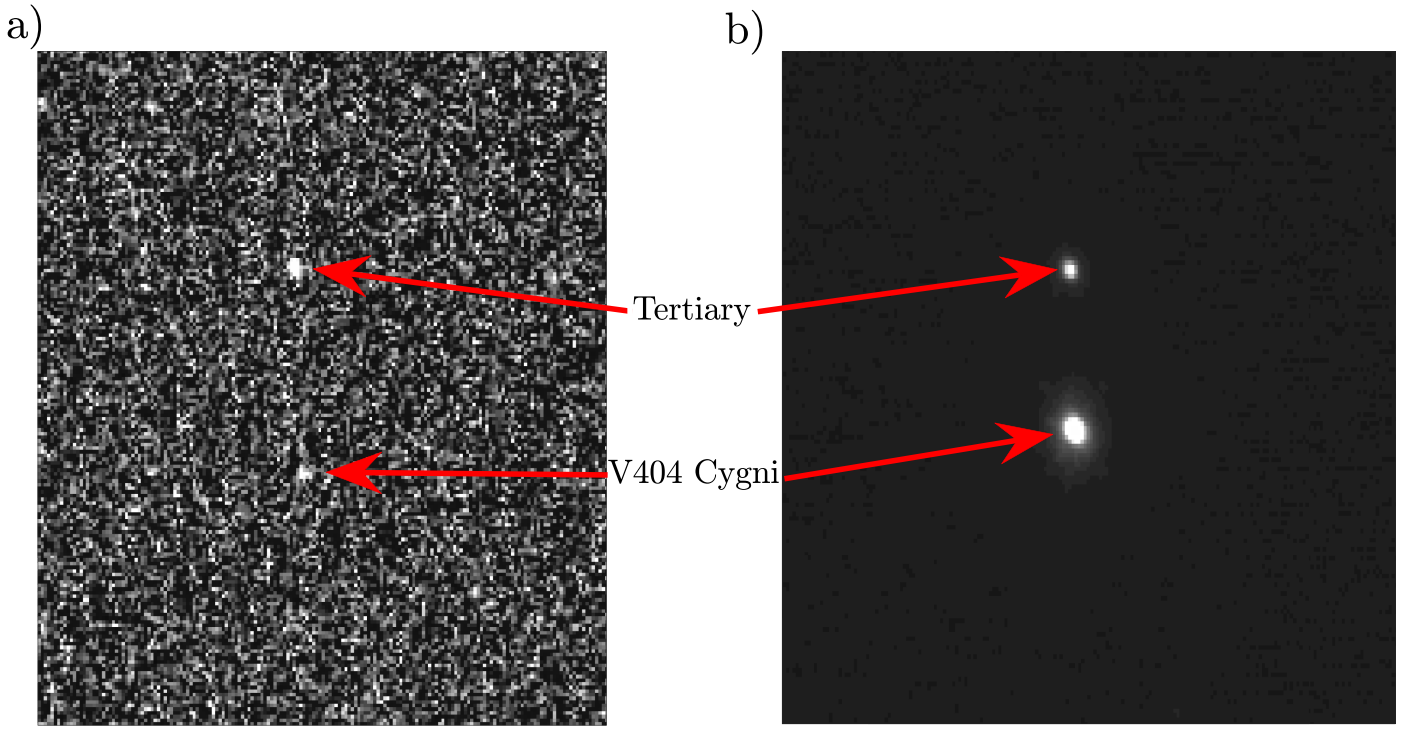

Extended Data Fig. 6 | High-resolution Hubble Space Telescope and Keck adaptive optics images of V404 Cygni and the tertiary. a, A Hubble Space Telescope ACS/HRC F330W image of V404 Cygni, with both objects labelled. We used this archival image to extract flux in the F330W filter, which was included in our analysis of the SED of the object. **b**, A Keck NIRC2 adaptive optics image obtained in the K_p filter, used in our analysis of the SED of the object.

Extended Data Table 1 | Gaia astrometry of V404 Cygni and the tertiary

Object	RA (epoch 2016)	Dec (epoch 2016)	ω	$\mu_{\rm RA}$	$\mu_{\rm Dec}$
V404 Cygni	306.0159085525	33.8671768648	0.3024 ± 0.0783	-5.1775 ± 0.0785	-7.7776 ± 0.0922
Tertiary	306.0159299085	33.8675732739	0.1423 ± 0.1161	-5.1500 ± 0.1564	-7.7647 ± 0.1316

We note that the Gaia parallax measurement is much less precise than the radio parallax of $\omega = 0.418 \pm 0.024$ reported in ref. 22. The proper motions are consistent with what was measured in the radio.